





Cite this: *Phys. Chem. Chem. Phys.*,  
2021, **23**, 15702

# In-flow optical characterization of flame-generated carbon nanoparticles sampled from a premixed flame†

F. Migliorini,<sup>a</sup> S. Belmuso,<sup>b</sup> S. Maffi,<sup>a</sup> R. Dondè <sup>a</sup> and S. De Iuliis <sup>\*a</sup>

In this work, the optical absorption properties of carbon nanoparticles are investigated by applying in-flow extinction and laser-induced incandescence measurements. Carbon nanoparticles are produced in an ethylene/air premixed flame and sampled at different heights above the burner. From extinction measurements, the absorption coefficient is obtained in a wide spectral range, considering the negligible scattering under our experimental conditions. With the application of Tauc plot the optical band gap is evaluated at the sampling heights under analysis. The increase of this value with the decrease in the height is consistent with the quantum confinement effect detected in the inception region of the flame. Two-color laser induced incandescence measurements are performed at relatively high laser fluence. The fluence curves, given by the particle temperature under laser irradiation *versus* laser fluence, are also obtained. A significant difference in the optical properties of these particles is observed by changing the sampling height. Moreover, considering the fluence curve in the low laser fluence regime, the refractive index absorption function  $E(m)$  is evaluated at an excitation wavelength of 1064 nm. Finally, the knowledge of the behavior of the absorption coefficient in a wide spectral range allows retrieving the values and the behavior of  $E(m)$  as a function of wavelength.

Received 22nd March 2021,  
Accepted 23rd June 2021

DOI: 10.1039/d1cp01267c

[rsc.li/pccp](http://rsc.li/pccp)

## 1. Introduction

Carbon nanoparticles or soot resulting from incomplete combustion processes have been widely investigated by the scientific community with the aim to assess their impact on human health and the environment.<sup>1,2</sup> From a different point of view, these nanoparticles can be considered a combustion by-product to be employed and enhanced in several different applications, spanning from gas sensing to electronics.<sup>3</sup> Interest in carbon nanoparticles is dictated by their specific physico-chemical properties essentially related to their structure and composition or maturity, given by their C/H ratio.<sup>4–8</sup> Being synthesized in flames, their properties are strongly dependent on fuel type and combustion conditions. These parameters can vary depending on the different stages of particle formation, from inception, coalescence or coagulation, surface growth and agglomeration.<sup>9–16</sup> Particles consist of large disordered molecular structures with sp, sp<sup>2</sup>, and sp<sup>3</sup> carbon hybridization. In particular, nascent particles are essentially characterized by sp<sup>2</sup>-bonded rings, which become large clusters with more ordered fine structure in mature carbon particles.

Moreover, knowledge of the optical properties of these carbon nanoparticles is also important for the application of optical diagnostics both for the study of particle formation mechanisms in flames<sup>12,17–21</sup> and *ex situ* for the characterization of these nanoparticles in terms of particle dimension and concentration.<sup>22</sup>

In recent years, increasing interest has been given to nascent carbon particles produced in premixed hydrocarbon flames and in particular those detected in the early stages of their formation. This interest is due to the peculiar properties of these nanoparticles, which have been found to be strongly dependent on their dimensions. In fact, due to a confinement effect,<sup>23,24</sup> reducing the size of the particles to a few nanometers results in different absorption and fluorescence features being observed.<sup>25</sup> In order to shed light on the composition of these structures and their properties, different diagnostic techniques and theoretical approaches have been implemented.<sup>23,26–28</sup>

UV-Vis absorption measurements are reported in the literature, with the aim to evaluate with a high accuracy the optical band gap (OBG) of these structures through a Tauc plot.<sup>29</sup> The application of this fundamental physical parameter, normally used for semiconductors, is extended to the description of the particles under analysis, which are considered to be amorphous carbon to some extent.<sup>30,31</sup> The optical band gap depends on the different hybridization of the carbon atom wave functions,

<sup>a</sup> CNR-ICMATE, Institute of Condensed Matter Chemistry and Technologies for Energy, Via R. Cozzi 53, 20125 Milan, Italy. E-mail: [silvana.deiullis@cnr.it](mailto:silvana.deiullis@cnr.it)

<sup>b</sup> Institute of Sciences and Technologies for Sustainable Energy and Mobility, Piazzale Tecchio 80, Naples 80125, Italy

† In memory of Silvia Maffi.



$sp^3$  and  $sp^2$ ,  $sp$  being considered absent in these systems, and in particular it is given by  $\pi-\pi^*$  energy transitions.<sup>30</sup>

The expression of the Tauc plot is different for the direct and indirect allowed transitions. For the particles under analysis, the choice between these two transitions is still an unresolved issue.

According to the work reported in ref. 32 and 33, analysis of the Tauc plot of the absorption spectra of nascent soot proves the indirect nature of the energy transition. Nascent particles sampled from ethylene/air premixed flames under different flame conditions (equivalence ratio, C/O ratio) were characterized by optical band gap values in the range of 0.7–2 eV. Moreover, OBGs were found to increase with a decrease in particle size. This quantum confinement behavior confirms the quantum dot nature of the particles under study. On the contrary, Miller and co-workers<sup>34</sup> assumed a direct transition for extinction measurements in non-premixed flames. They obtained OBG values in the range of 1.8–2.35 eV, and attributed these values to PAH of 14 rings.

Actually, apart from a few measurements on the characterization of these particles (fluorescence and photoelectron emission), more work is needed to gain comprehensive knowledge and a description of their structure and, as a consequence, of their properties. For instance, information about the refractive index and the resulting refractive index absorption function  $E(m)$  are very limited, and this is also an important issue for optical measurements.

In this work, nanoparticles produced in an ethylene/air premixed flame are sampled and characterized in the flow. UV-Vis extinction and laser-induced incandescence measurements are carried out. The aim is to develop a suitable tool for fast analysis of the optical properties of the nanoparticles before collection for possible easy post-treatment of these particles. Moreover, the approach proposed avoids possible artefacts due to off-line measurements on plate-deposited particles. In order to discriminate the contribution of

gaseous species to the total absorption spectra, a glass fiber filter is used in order to stop the particle flow in the measuring tube. Laser-induced measurements are performed by means of an in-house developed LII instrument (SILIIS).<sup>22</sup> In particular two-color LII was performed at a relatively high laser fluence changing the sampling height of the particles under analysis. Moreover, LII measurements have been performed at each height by varying the laser fluence, in order to investigate the behavior of the particle temperature under laser irradiation as a function of the laser energy density used. These results provide information on the optical/incandescence properties of these nanoparticles. Finally, by combining absorption and incandescence measurements, the refractive index absorption function  $E(m)$  is obtained in the spectral range under analysis.

## 2. Experimental setup

The experimental set-up employed for extinction measurements is reported in Fig. 1.

Measurements have been carried out on carbon nanoparticles produced and sampled from a rich premixed ethylene/air flame. To this aim, a bronze McKenna burner is used, which is proved to produce homogeneous composition and temperature radially across the flame. This burner is considered to produce reference flames for calibration purposes. A stainless-steel plate of 60 mm diameter, located at a height of 30 mm above the burner, is used to stabilize the flame. In this work the outer  $N_2$  flow is not used to shield the flame.

Measurements were performed with flow rates for ethylene and air fixed at  $2.38 \text{ l min}^{-1}$  and  $14.6 \text{ l min}^{-1}$ , respectively, resulting in an equivalence ratio of  $\varphi = 2.3$  and  $C/O = 0.77$ . The gas velocity was  $10 \text{ cm s}^{-1}$ .

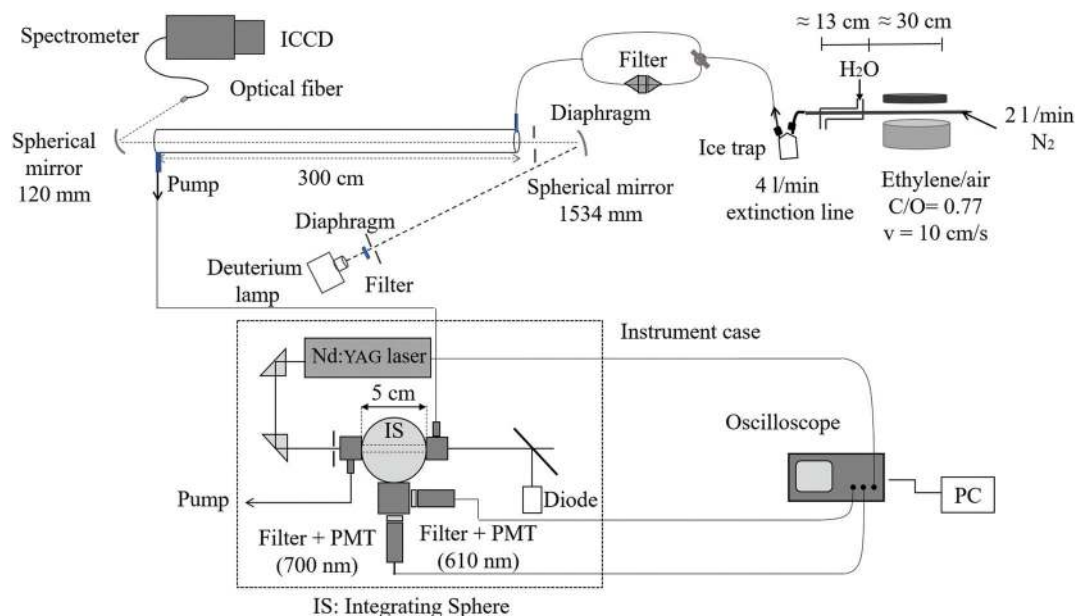


Fig. 1 Experimental set-up: synthesis flame, a measuring tube for extinction measurements and an in-house developed LII instrument.



In order to collect carbon nanoparticles at different heights, the burner was mounted on a motorized translation stage that moves the burner both vertically and horizontally. In this work the following sampling heights (SH) are considered: 4 mm, 5 mm, 6 mm, 7 mm, 8 mm, 10 mm and 14 mm.

The particles are sampled from the center of the flame through a 2 mm diameter hole of a horizontal stainless-steel sampling probe (10 mm O.D. and 8 mm I.D.) into the measuring cell. In order to quench the chemical reactions, nitrogen is flowing in the sampling probe. Values of  $2 \text{ Nl min}^{-1}$  of  $\text{N}_2$  and  $4 \text{ Nl min}^{-1}$  of the pumping systems are used as a compromise to quench and dilute the aerosol under analysis, still maintaining good sensitivity in the absorption measurements. During the experiments, in order to monitor the clogging of the sampling inlet due to particles, the pressure drop is measured with a pressure transducer (SETRA 239). Thermal conditions are also controlled by measuring the gas temperature inside the sampling tube with a thermocouple. An ice trap unit is used to remove combustion water vapor from the sample.

Moreover, in order to evaluate the contribution of the gas phase to the absorption measurements of the particles present in the aerosol, a glass fiber filter (Whatman,  $\varnothing = 47 \text{ mm}$ ) is positioned before the measuring cell, which is however bypassed for total absorption measurements.

## 2.1 Extinction

For extinction measurements, the carbon nanoparticles sampled from the flame are sent into a measuring cell. The cell consists of a 300 cm cylindrical polycarbonate tube closed at its ends with two quartz windows (50 mm diameter). To this purpose, in order to remove chromatic effects, a schlieren mirror is used with a focal length of 1534 mm. The light beam, after passing in the tube, is focused on an optical fiber (Oriel, 3 mm bundle diameter) by means of a second spherical mirror (120 mm focal length).

In order to cover the spectral range from UV to early IR, different set-ups are employed.

- In the 240–400 nm spectral range a deuterium lamp (63379 Oriel 30 W) is used as a light source. A portion of the light emitted from the lamp is selected with a diaphragm (aperture = 3.2 mm) and collimated into the measuring cell. To detect the signal intensity in the UV spectral range, an intensified 1024 element diode array (Tracor Northern, TN-6130-1, 0.6 nm resolution) is employed.

- In the second range (300–700 nm) the same light source is used, while the signal intensity is measured with a Czerny–Turner spectrograph (Shamrock 303i) coupled with an ICCD camera (iStar 334T, Andor Technology), the spectral response of this spectrometer being more efficient in the visible/near IR spectral range. For these measurements a low-resolution grating (150 grooves per mm) is adopted. This spectrometer is employed to also measure signals in the other spectral ranges reported in the following.

- At longer wavelengths (600–850 nm) we change the light source with an intense diffuse halogen lamp (400 W).

- Finally, in order to measure the absorption coefficient at a wavelength of 1064 nm, a cw Nd:YVO<sub>4</sub> laser is employed,

not reported in the figure to maintain clarity. This laser was pumped by means of a diode laser at about 800 nm, and this line was also used for the extinction measurements.

The final absorption spectra are obtained by matching consecutive spectral ranges, taking advantage of the small superimposition of the wavelengths. Moreover, in order to remove second order contributions, high pass filters are alternately positioned just in front of the light source employed.

In order to improve the signal to noise ratio, each signal results from an accumulation of 500 spectra.

The extinction measurements are performed as follows. As a first step, we measure the spectral emission from the light source with the sampling line outside the flame and the glass fiber filter before the measuring cell. Then, after sampling the aerosol from the flame, the transmitted light across the tube is measured in the total spectral range under analysis, alternately with and without the glass fiber filter. In this way, the gas and the total aerosol extinction can be obtained, and from these spectra, the only contribution of the particles to the extinction can be retrieved.

## 2.2 Laser-induced incandescence

For laser-induced incandescence measurements, a portable in-house developed instrument is used.<sup>22</sup> The sphere-integrated LII spectroscopy instrument (SILIIS) is essentially based on a two-color LII technique. A portion of the aerosol sampled from the flame, after passing across the extinction measuring tube, is pumped into the SILIIS instrument, as shown in the figure. Details of the instrument are given in ref. 22. In particular, the measuring cell consists of a quartz tube (I.D. = 6.7 mm, O.D. = 9 mm, and 10 cm long) closed with two quartz windows at each end. The IR Nd:YAG laser beam (Quantel, Big Sky, CFR 400) is properly aligned to the cell. A portion of the laser beam is selected in order to prevent laser scattering from the walls. The test cell is placed inside an integrating sphere (Sphere Optics Hoffman LLC, Contoocook, NH, USA), used in order to increase the detection sensitivity. The LII signal is collected and measured with two photosensor blocks (Hamamatsu) in front of which two bandpass filters at 610 nm (FWHM = 40 nm) and 700 nm (FWHM = 60) are positioned, respectively.

For these measurements the filter at 610 nm is chosen instead of 530 nm, which is normally used in the instrument. The choice of the two wavelengths aims to reduce the uncertainty of temperature measurements using two-color pyrometry, as reported by Liu *et al.*<sup>35</sup> Time-resolved incandescence signals at the two spectral ranges are detected with a fast-digital oscilloscope (Agilent Technologies, MS06104A, 1 GHz, 4 Gs s<sup>-1</sup>). Each signal is taken with an average over 256 curves. The “prompt” signal is obtained with a gatewidth of 4 ns on the peak of the LII signal (1 ns before and 3 ns after the maximum). In order to avoid the occurrence of multiple laser pulses, a flow rate of  $1 \text{ Nl min}^{-1}$  and a laser frequency of 5 Hz are used.<sup>36–38</sup>

Measurements have been performed at high laser fluence ( $350 \text{ mJ cm}^{-2}$ ) on carbon nanoparticles sampled at different SHs. Moreover, at SH = 7 mm, 8 mm, 10 mm and 14 mm, two-color LII signal is detected by changing the laser fluence.



### 3. Results

#### 3.1 Absorption measurements of aerosol particles

According to the Beer–Lambert law, the spectral transmittance  $\tau_\lambda$ , given by the ratio of transmitted  $I_{\lambda,T}$  and incident  $I_{\lambda,0}$  light intensity for each wavelength  $\lambda$ , can be expressed as

$$\tau_\lambda = \frac{I_{\lambda,T}}{I_{\lambda,0}} = \exp\left(-\int_0^L k_{\text{ext},\lambda} dx\right) \quad (1)$$

where  $k_{\text{ext},\lambda}$  is the extinction coefficient of the particles in the aerosol,  $x$  is the spatial location along the extinction pathway, and  $L$  is the optical pathlength. If the distribution of the aerosol inside the tube is considered to be uniform, eqn (1) can be written as:

$$-\ln \tau_\lambda = k_{\text{ext},\lambda} L \quad (2)$$

The extinction coefficient is expressed as  $k_{\text{ext},\lambda} = k_{\text{abs},\lambda} + k_{\text{scatt},\lambda}$ , where  $k_{\text{abs},\lambda}$  and  $k_{\text{scatt},\lambda}$  are the wavelength-dependent absorption and scattering coefficients, respectively. If the scattering contribution can be considered to be negligible, the transmittance measurements give the direct measurement of absorption coefficient. In our case, where nanoparticles at the first stages of their formation are probed, the single scattering albedo (defined as the scattering coefficient over the extinction coefficient) can be neglected as clearly reported in ref. 20. In fact, in this work, scattering and extinction measurements were performed in the same flame, under the same experimental conditions (C/O – equivalence ratio, and ethylene/air) but with different gas velocity and different position of the stabilizing plate (20 mm instead of 30 mm as in this work). By investigating the flame along its axis, the scattering coefficient was found to be about three orders of magnitude lower than extinction, for all the heights under analysis. For this reason, we are confident in neglecting the scattering albedo even in our measurements, and consequently in considering extinction being equal to the absorption coefficient.

The absorption coefficient is related to the volume concentration of the particles in the probe volume through this relationship

$$k_{\text{abs},\lambda} = \frac{6\pi E(m) f_V}{\lambda} \quad (3)$$

where  $E(m)$  is a function of the refractive index of the particles. According to eqn (3), from extinction measurements once the wavelength dependence of the absorption coefficient is obtained, the optical properties of these nanoparticles can be derived.

As already described in the previous section, the particle absorption coefficient is obtained by correcting the total aerosol absorption with the contribution of the gas phase. For measurements at a height lower than 5 mm, the particle absorption coefficient is actually negligible, at least under our experimental conditions, where the total absorption coefficient is essentially given by the gas contribution.

In Fig. 2 the particle absorption coefficient is reported *versus* wavelength for the sampling heights under analysis. The uncertainty of these measurements is evaluated to be 11%. The spectra exhibit a significant change in the intensity as well as in the wavelength-dependence with the decrease of the height up to 5 mm.

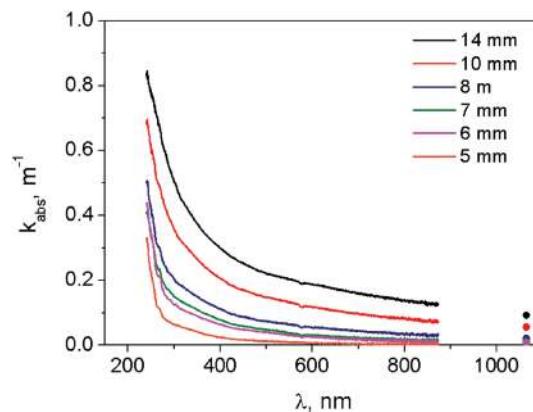


Fig. 2 Absorption coefficient *versus* wavelength at several sampling heights.

Considering the impact of the gas on the total absorption, we report in Fig. 3 the absorption coefficient of the gas-phase species *versus* wavelength for the SHs under analysis.

As is evident, this contribution is negligible for wavelengths longer than 300 nm. On the contrary, for shorter wavelengths, the gas absorption coefficient cannot be neglected, resulting in an increase with the decrease in the sampling height. In particular, in this region two peaks can be observed at about 250 nm and 270 nm, which can be attributed to the presence of organic compounds and in particular polycyclic aromatic hydrocarbons, which are known to exhibit broad absorption bands in the UV spectral range.<sup>39</sup>

In order to investigate the main differences in the absorption coefficient of the particles under analysis changing the sampling height, the  $k_{\text{abs},\lambda}$  spectra are fitted by using a power law function. In particular the empirical relation proposed in ref. 40  $k_{\text{ext},\lambda} = c\lambda^{-\alpha}$  is used, where  $c$  is a function of the particle concentration and  $\alpha$  is the dispersion exponent. In the literature different spectral ranges are used for the fitting. Just to mention some examples, in the work of Russo *et al.*<sup>33</sup> as well as in the work of Simonsson *et al.*,<sup>12</sup> the fitting is performed in the spectral range of 685–1064 nm. The choice aims to emphasize the contribution of the soot-like behavior to the incipient carbon particles. Moreover, in the

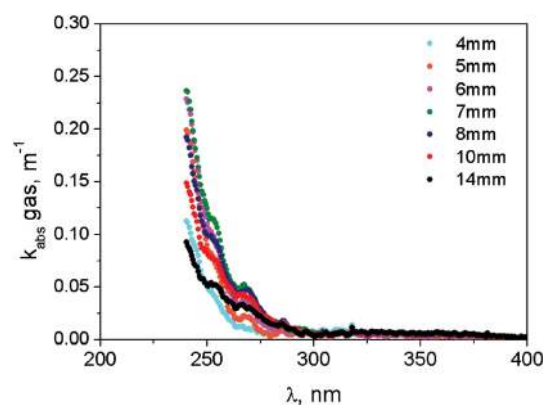


Fig. 3 Absorption coefficient of gas-phase species *vs.* wavelength at different SHs.



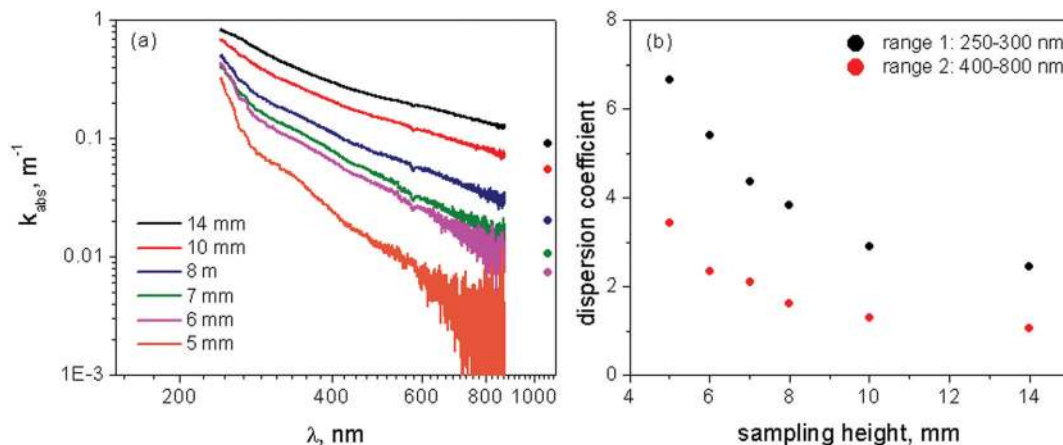


Fig. 4 (a) Absorption spectra in logarithmic scale at different SHs. (b) Dispersion coefficient versus sampling height calculated in the two spectral ranges, namely 250–300 nm and 400–800 nm.

work of Minutolo *et al.*<sup>32</sup> in agreement with that of Millikan,<sup>40</sup> the spectral range of 400–600 nm is chosen for the fitting.

We report in Fig. 4a the absorption spectra in logarithmic scale in order to emphasize the change of the dispersion exponent with the wavelength.

The spectra are characterized by a quick decrease in the low spectral range and a wide tail at longer wavelengths. Such behavior can hardly be described by a single power law along the spectral range under analysis. For this reason, two different spectral ranges are considered to fit the experimental spectra, namely 250–300 nm and 400–800 nm. In Fig. 4b the resulting values of the dispersion exponent as a function of the SH are reported.

In both ranges, the value of the dispersion exponent increases with the decrease of SH, in agreement with the trends reported in the literature. Obviously, the values are different from the literature data as different spectral ranges are considered for the fitting. The high values of the dispersion exponent are attributed to incipient carbon nanoparticles with larger H/C ratios in agreement with the work of Minutolo *et al.*<sup>32</sup> This result proves the significant changes in the optical properties of the particles sampled from the flame at different heights, which is attributed to changes in the structural and chemical composition of the particles under analysis.

### 3.2 Optical band gap

According to Tauc and Davis and Mott,<sup>29,41</sup> the optical band gap can be calculated from this relationship:

$$h\nu \times k_{\text{abs},\lambda} \sim (h\nu - E_g)^r \quad (4)$$

where  $k_{\text{abs},\lambda}$  is the absorption coefficient and  $r$  is a constant depending on the particular optical transition. Considering eqn (3), OBG can be experimentally retrieved by plotting  $k_{\text{abs},\lambda}$  as a function of the energy and extrapolating the linear slope to zero absorption. This is possible once the value of  $r$  is known. Considering an allowed transition, the value is  $r = 1/2$  or 2 for direct and indirect transition, respectively. The nature of the transition for the particles under analysis is still under debate in the combustion community and could also be dependent on

the particular nascent carbon particles considered. Moreover, we have to stress that the data reported in this work refer to the absorption coefficient of particles in an aerosol, which could be different compared to the results obtained after film deposition on a quartz/glass plate. In agreement with the work of ref. 32, an indirect transition is considered for the nanoparticles under study, as also confirmed by theoretical calculations of  $\pi$ - $\pi^*$  energy transition in large aromatic clusters.<sup>24,42</sup>

We report in Fig. 5a examples of  $\sqrt{h\nu \times k_{\text{abs},\lambda}}$  as a function of the photon energy  $E$ , with the corresponding linear fitting curves for OBG evaluation.

The optical band gap here obtained can be attributed to the presence of structures with significant  $sp^2$  aromatic clusters and in particular to the corresponding  $\pi$ - $\pi^*$  interactions.

In Fig. 5b we report the values of the OBG as a function of the sampling height, compared with the data from ref. 11 and 33. Our values of OBG are reasonably in agreement with the values taken from the literature, referring to both *ex situ* and *in situ* measurements. As can be seen, by decreasing this height an increase of the optical band gap is obtained. If one considers that a decrease in the particles size is detected at a lower height (see for example ref. 20), the plot seems to be consistent with the quantum confinement effect observed at a low height in the flame.<sup>24</sup>

### 3.3 Laser-induced incandescence measurements

Further analysis of the difference in the optical properties of nanoparticles sampled at different heights is performed by investigating their response to laser irradiation. Two-color laser-induced incandescence measurements are carried out at relatively high laser fluence ( $350 \text{ mJ cm}^{-2}$ ) as a function of the height. For brevity, we report here only a few formulae used in the following. We refer the reader to other published literature studies for more in-depth descriptions.<sup>35,43</sup>

The incandescence signal intensity  $I_{p,\lambda}$  emitted at a given wavelength  $\lambda$  by a concentration of particles  $f_V$  heated at a temperature  $T_p$  is given by the following relationship:

$$I_{p,\lambda}(T_p, f_V) = \eta_{\lambda} R_{\text{BB}}(T_p, \lambda) \varepsilon(\lambda) \quad (5)$$



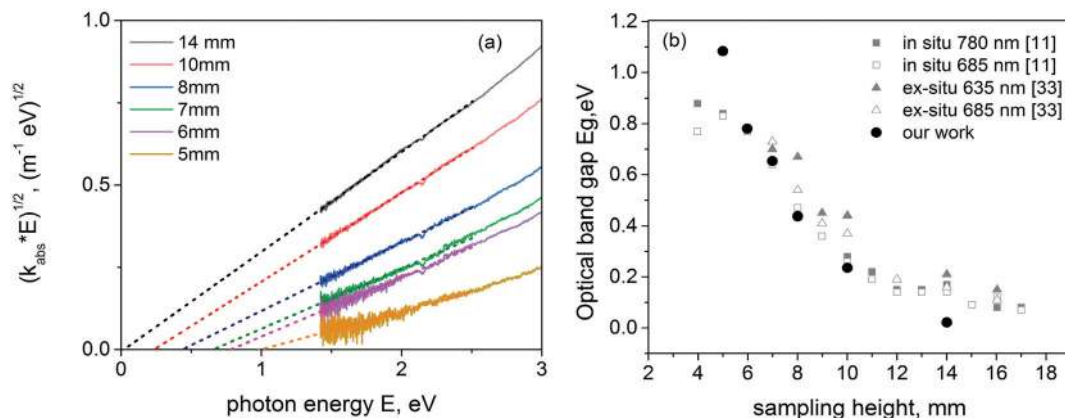


Fig. 5 Examples of Tauc plot with the fitting procedure to evaluate OBG (a). Optical band gap versus sampling height and comparison with data in the literature<sup>11,33</sup> (b).

where  $R_{\text{BB}}$  is the blackbody energy spectral density, as given by Planck's law,  $\varepsilon(\lambda)$  is the monochromatic emissivity and  $\eta_\lambda$  is the detection efficiency coefficient. Assuming the Wien approximation to be valid, the blackbody energy spectral density can be expressed as:

$$R_{\text{BB}}(T_p, \lambda) \propto \frac{1}{\lambda^5} \frac{\varepsilon(\lambda)}{\left( e^{\left( \frac{hc}{\lambda k T_p} \right)} - 1 \right)} \sim \frac{1}{\lambda^5} e^{\left( \frac{hc}{\lambda k T_p} \right)} \quad (6)$$

where  $h$  is the Planck constant,  $k$  is the Boltzmann constant and  $c$  is the speed of light. Assuming Kirchhoff's law to be valid, soot emissivity can be related to absorption coefficient through the following relationship:

$$\varepsilon(\lambda) = 1 - \exp(-k_{\text{abs},\lambda} L) \quad (7)$$

where  $L$  is the length of the homogeneous probe volume. By applying the pyrometry approach,<sup>35</sup> incandescence temperature is retrieved thanks to a calibration procedure performed with a calibrated tungsten lamp. In particular, for these measurements the same calibration procedure reported in the work by Migliorini *et al.* is applied.<sup>22</sup>

In order to take into account the optical properties of the particles under analysis, which significantly change with the sampling height, the wavelength-dependent absorption coefficient obtained here is used. In fact, according to eqn (3), the ratio of the absorption coefficient in the two spectral ranges gives directly the ratio of  $E(m)$  at the two wavelengths, for each SH.

By measuring the incandescence signal at two wavelength ranges,  $\Delta\lambda_1$  and  $\Delta\lambda_2$ , the expression of particle temperature  $T_p$  can be retrieved as:

$$T_p = \frac{hc}{k} \left( \frac{1}{\lambda_2} - \frac{1}{\lambda_1} \right) \left[ \ln \left( \frac{I_{p,\lambda_1} \eta_{\lambda_2} \Delta\lambda_2 k_{\text{abs},\lambda_2} \left( \frac{\lambda_1}{\lambda_2} \right)^5}{I_{p,\lambda_2} \eta_{\lambda_1} \Delta\lambda_1 k_{\text{abs},\lambda_1} \left( \frac{\lambda_2}{\lambda_1} \right)} \right) \right]^{-1} \quad (8)$$

In Fig. 6 the peak of the incandescence temperature is reported versus SH. The corresponding uncertainty has been estimated considering both the uncertainty in the incandescence signal

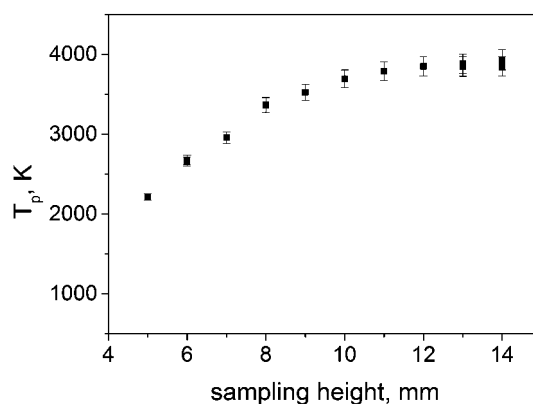


Fig. 6 The peak of incandescence temperature versus sampling height and corresponding uncertainty at 350 mJ cm<sup>-2</sup> laser fluence.

(3% relative error) and that of the ratio of the absorption coefficient (4% relative error), which results in being 7% maximum. For the sampling heights where no extinction measurements were performed, the absorption coefficient has been evaluated by means of linear interpolation between close values.

Although for these measurements a high laser fluence is used, the peak of the incandescence temperature continues to increase with SH, reaching a plateau only at the higher values of SH analyzed. This behavior is in agreement with the results reported in ref. 11 and 44, however it is different compared to the classical response of the incandescence temperature of carbon particles in the high laser fluence regime. This is clearly related to the significantly different nature of the particles changing the sampling height. For this, care has to be taken for the application of a laser-induced incandescence technique for volume fraction measurements. Moreover, at the same time more insights into the nature of the optical properties of these nanoparticles can be obtained by looking at the response of these nanoparticles under laser irradiation at different laser fluence. We report in Fig. 7 the fluence curves, showing the incandescence temperature versus laser fluence, for SH = 7 mm, 8 mm, 10 mm and 14 mm. For lower sampling heights, it was



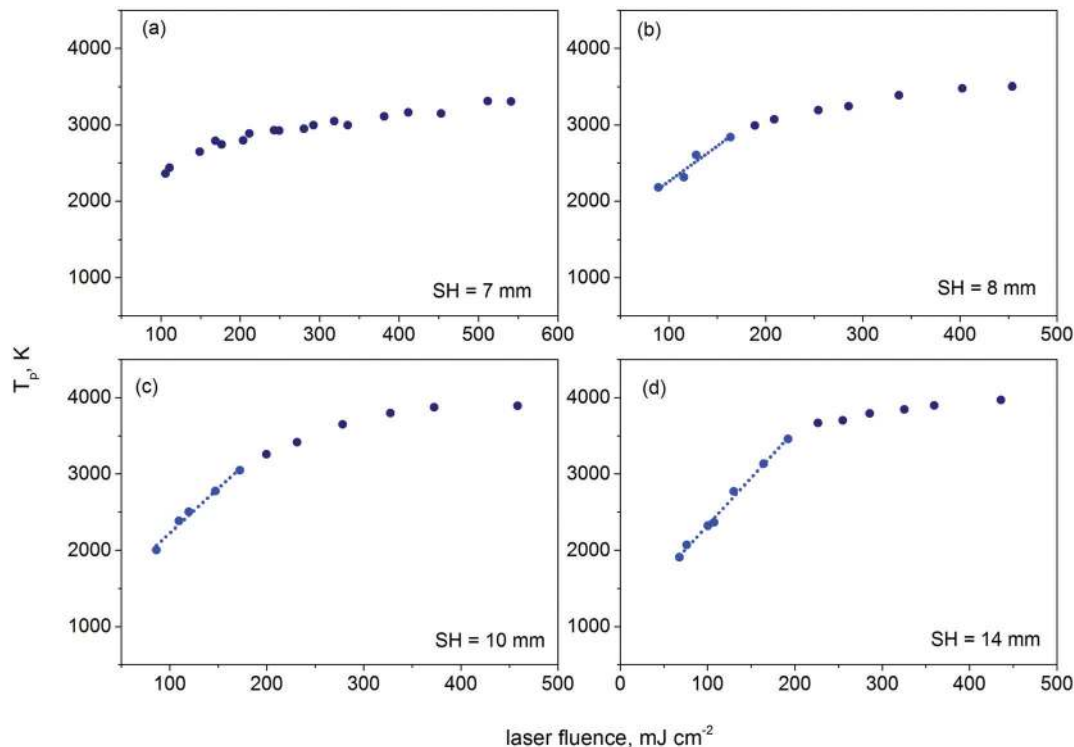


Fig. 7 Incandescence temperature vs. laser fluence at 7 mm (a), 8 mm (b), 10 mm (c) and 14 mm (d) (dark blue symbols). Light blue symbols refer to data points used for fitting (dotted lines).

difficult to obtain reliable fluence curves, as, due to the decrease in the particle concentration, low values of the incandescence signal were detected, especially at low laser fluence.

As can be seen, the behavior of the fluence curve changes significantly with SH. In particular, for a height of 14 mm the temperature increases almost linearly up to 200 mJ cm<sup>-2</sup>, above which a bending of the curve is detected with values of temperature slightly higher than 4000 K. It is really hard to see a plateau in this region. For lower heights, the bending of the fluence curve is less and less evident and, compared to the measurements at 14 mm, lower temperatures are reached at high laser fluence. A particular trend of the fluence curve is detected at 7 mm. Here the linear increase in the low laser fluence regime cannot be observed and temperature increases continuously up to 550 mJ cm<sup>-2</sup>. Unfortunately, moving to a lower sampling height, due to lower particle concentration, the minimum laser fluence at which temperature can be measured shifts to higher values.

The significant difference in the fluence curve can be attributed to the difference in the optical properties of the particles under analysis, which depend on their inner chemical structure. One would expect a different response of these nanoparticles to the laser irradiation due to a probably different effect and change in their properties.

## 4. Discussion

In principle, considering the fluence curve, an estimation of the refractive index absorption function  $E(m)$  can be derived by

looking at the behavior of the temperature of particles under laser irradiation in the low laser fluence regime. Here, the incandescence peak temperature ( $T_p$ ) of the carbon nanoparticles is related to the gas temperature ( $T^0$ ) and to the laser fluence ( $F$ ) through the following linear relationship:<sup>43</sup>

$$T_p - T^0 = \frac{6\pi E(m)F}{\lambda_{\text{exc}} c_p \rho_p} \quad (9)$$

where  $E(m)$  depends on the optical properties of the particles under analysis,  $c_p$  is the heat capacity and  $\rho_p$  is the particle density. The difference in the particle temperature linearly depends on the laser fluence  $F$ , and the slope of such dependence is strictly related to the optical properties. Other approaches to retrieve the refractive index absorption function are reported in the literature.<sup>45,46</sup>

We apply eqn (9) to the fluence curves obtained at SH = 8 mm, 10 mm and 14 mm, where a linear trend is clearly shown in the low fluence regime. Considering the slope of the linear curve the values of  $E(m) = 0.23, 0.28,$  and  $0.3$  at 1064 nm excitation wavelength are obtained for SH = 8 mm, 10 mm and 14 mm, respectively. For this evaluation, we use the value of the product of the specific heat capacity and particle density proposed by Michelsen.<sup>47</sup> In this work, in fact, it was shown that while the specific heat decreases, the density increases with C/H, which means with soot maturity. Correspondingly, the product of specific heat and density is independent of C/H. For this reason, we use the same value for the different heights above the burner. According to eqn (9), the intercept of the



linear fitting should give the initial temperature of the particle before the laser was shot. However, temperature values higher than ambient temperature are obtained in our case. This means that if the particles are irradiated by the laser at significantly low laser fluence (approaching zero value) they are heated up from ambient temperature to a significantly high incandescence temperature. Then, a steeper slope in the fluence curve should occur, resulting in a higher value of  $E(m)$  or, alternatively, a lower value of the product of the heat capacity and density of the carbon nanoparticles under analysis. In our opinion, a modification of the optical properties of these nanoparticles could occur, and such modification might be dependent on the initial structure of the nanoparticles under analysis. In brief the modification of the carbon nanoparticles due to the heating process could not be neglected even at very low laser fluence. As a further point to consider to explain such an effect, in pyrometry the signal intensity is biased towards the highest value of temperature. Then, any non-uniformity of the fluence in the probe volume would result in an overestimation of the particle temperature. This effect is partially responsible for a decrease of  $f_V$  with the decrease in the laser fluence (the so-called “soot volume fraction anomaly”).<sup>48</sup> Unfortunately, this phenomenon is far from completely understood. More work is needed to shed light on these issues.

For the fluence curve at SH = 7 mm, it is really difficult to find a linear trend in the low laser fluence regime, which confirms the definitely different nature and composition of the particles at this SH.

By coupling absorption and incandescence measurements, the dependence of the refractive index absorption function can be estimated as a function of wavelength. In fact, considering the values of  $E(m)$  evaluated from the fluence curves at 8 mm, 10 mm and 14 mm, the estimation of  $E(m)$  in a wide spectral range are derived by scaling absorption coefficient multiplied by wavelength, according to eqn (3). In Fig. 8, the behavior of  $E(m)$  versus wavelength is shown for SH = 8 mm, 10 mm and 14 mm.

At 8 mm sampling height a strong decrease of  $E(m)$  is detected by increasing the wavelength, which is more significant in the UV spectral region. Moving to higher sampling heights, for a wavelength shorter than 400 nm this slope in the  $E(m)$  curve is reduced and the behavior at longer wavelengths tends to flatten. Finally at 14 mm in the visible/near IR region the values of  $E(m)$  can be considered almost constant with the wavelength.

The overall trend of  $E(m)$  with wavelength is in agreement with the results by Bescond *et al.*<sup>5</sup> They performed UV-visible-near IR extinction measurements to investigate the optical properties of nanoparticles produced by means of a miniCAST, an ethylene diffusion flame and a PALAS. By coupling these results with mass concentration measurements *via* a tapered element oscillating microbalance, they were able to retrieve the refractive index absorption function also, thanks to the application of RDG-FA theory. Obviously, the physico-chemical properties of nanoparticles produced with the diffusion flame and the PALAS are very different from our case. On the contrary, comparing our  $E(m)$  values with miniCAST results, a good

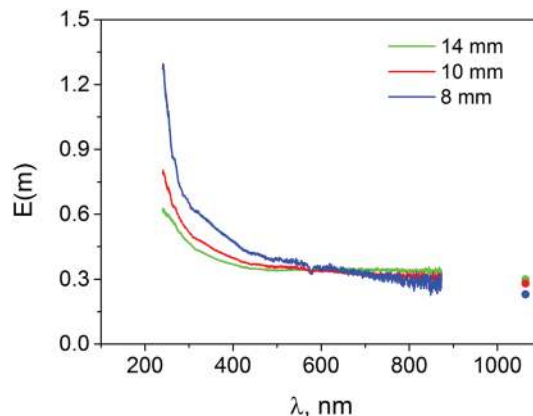


Fig. 8 Refractive index absorption function versus wavelength for SH = 8, 10, and 14 mm.

agreement is obtained on the overall spectral trend even considering the different experimental conditions employed. In fact, in the miniCAST propane is used as a fuel in a diffusion flame, where however different OC/TCs can be selected. The unexpected behaviour detected at a wavelength shorter than 600 nm (more mature particles exhibiting higher  $E(m)$  values) might be due to the different nature of the nanoparticles at the sampling heights under analysis.

Absolute values of  $E(m)$  at 1064 nm are also given by Olofsson *et al.* as obtained with two-color LII measurements and Lund modelling under IR laser irradiation.<sup>11</sup> They retrieved this value at different heights above the burner. Although the experimental conditions are not exactly the same (same equivalence ratio, and the same gas velocity but different stabilizing plates) the values obtained at 8, 10, and 14 mm are reasonably in agreement with our results. Good agreement is also obtained with the results from ref. 44–49. However, it is important to stress that, while in the studies published in ref. 11 and 44–49 measurements were carried out in a flame, in our case particles sampled from the flame were investigated at ambient temperature. The wide variation of  $E(m)$  in the flame accounts for the strong evolution of the physical and chemical structure of these nanoparticles. This could be very useful from a materials science point of view. In fact, with a proper choice of the sampling height, it is possible to collect particles having specific optical properties, which might be of great interest in different applications.

## 5. Conclusions

In this work carbon nanoparticles produced in an ethylene/air premixed flame are sampled and characterized in flow by means of UV-Vis-NIR absorption and laser-induced incandescence measurements. Particles are sampled at different heights starting from the inception region of the flame. The analysis is performed in flow, in order to avoid possible artefacts due to on-plate absorption measurements. The contribution of gas-phase species is evaluated and considered to determine the absorption of the particles under analysis. From these measurements and applying the Tauc plot for an indirect allowed transition, the optical band





gap is obtained, which increases up to 1 eV with the decrease of the sampling height. This is due to a reduction in the  $sp^2$  aromatic clusters going lower in the inception region. This behavior is also consistent with the confinement effect. Laser-induced incandescence measurements have been performed to indirectly investigate the absorption properties of these nanoparticles under IR laser irradiation. A different behavior of the temperature *versus* laser fluence is obtained for the different sampling heights in the flame. This is probably due not only to the different optical properties of these nanoparticles, but also to an effect of the laser in changing these properties. Therefore, care has to be taken in the application of this technique for particle concentration measurements. The analysis of the response of these nanoparticles to laser irradiation allowed us to gain information on the refractive index absorption function  $E(m)$  at the excitation wavelength. This is obtained by measuring the peak of the incandescence temperature *versus* laser fluence in the low laser fluence regime. Finally, from the absorption coefficient spectra and  $E(m)$  values at 1064 nm, the behavior of  $E(m)$  in a wide spectral range is derived. The wide change in the values of  $E(m)$  proves the strong evolution of the physical and chemical structures of these nanoparticles along the flame. This means that with an appropriate choice of sampling height, it is possible to collect particles of specific optical properties, which might be useful in different applications.

## Conflicts of interest

There are no conflicts to declare.

## Acknowledgements

The authors would like to acknowledge the financial support from the PRIN project 2017PJ5XXX: "Modeling and Analysis of carbon nanoparticles for innovative applications Generated directly and Collected During combustion (MAGIC DUST)".

## References

- C. A. Pope and D. W. Dockery, Health effects of fine particulate air pollution: Lines that connect, *J. Air Waste Manag. Assoc.*, 2006, **56**(6), 709–742, DOI: 10.1080/10473289.2006.10464485.
- T. C. Bond, *et al.*, Bounding the role of black carbon in the climate system: A scientific assessment, *J. Geophys. Res.: Atmos.*, 2013, **118**(11), 5380–5552, DOI: 10.1002/jgrd.50171.
- L. Xiao, H. Sun and L. Xiao, Nanoscale horizons novel properties and applications of carbon nanodots, *Nanoscale Horiz.*, 2018, **3**, 565–597, DOI: 10.1039/C8NH00106E.
- A. Baldelli, U. Trivanovic, T. A. Sipkens and S. N. Rogak, On determining soot maturity: A review of the role of microscopy- and spectroscopy-based techniques, *Chemosphere*, 2020, **252**, DOI: 10.1016/j.chemosphere.2020.126532.
- A. Bescond, *et al.*, Soot optical properties determined by analyzing extinction spectra in the visible near-UV: Toward an optical speciation according to constituents and structure, *J. Aerosol Sci.*, 2016, **101**, 118–132, DOI: 10.1016/j.jaerosci.2016.08.001.
- J. Yon, R. Lemaire, E. Therssen, P. Desgroux, A. Coppalle and K. F. Ren, Examination of wavelength dependent soot optical properties of diesel and diesel/rapeseed methyl ester mixture by extinction spectra analysis and LII measurements, *Appl. Phys. B: Lasers Opt.*, 2011, **104**(2), 253–271, DOI: 10.1007/s00340-011-4416-4.
- K. C. Le, T. Pino, V. T. Pham, J. Henriksson, S. Török and P. E. Bengtsson, Raman spectroscopy of mini-CAST soot with various fractions of organic compounds: Structural characterization during heating treatment from 25 °C to 1000 °C, *Combust. Flame*, 2019, **209**, 291–302, DOI: 10.1016/j.combustflame.2019.07.037.
- K. O. Johansson, F. El Gabaly, P. E. Schrader, M. F. Campbell and H. A. Michelsen, Evolution of maturity levels of the particle surface and bulk during soot growth and oxidation in a flame, *Aerosol Sci. Technol.*, 2017, **51**(12), 1333–1344, DOI: 10.1080/02786826.2017.1355047.
- E. Sutcu, *et al.*, Morphological and radiative characteristics of soot aggregates: Experimental and numerical research, *Sci. Rep.*, 2020, **10**(1), 1–33, DOI: 10.1038/s41598-019-57045-y.
- G. A. Kelesidis and S. E. Pratsinis, Soot light absorption and refractive index during agglomeration and surface growth, *Proc. Combust. Inst.*, 2019, **37**(1), 1177–1184, DOI: 10.1016/j.proci.2018.08.025.
- N. E. Olofsson, J. Simonsson, S. Török, H. Bladh and P. E. Bengtsson, Evolution of properties for aging soot in premixed flat flames studied by laser-induced incandescence and elastic light scattering, *Appl. Phys. B: Lasers Opt.*, 2015, **119**(4), 669–683, DOI: 10.1007/s00340-015-6067-3.
- J. Simonsson, N. E. Olofsson, S. Török, P. E. Bengtsson and H. Bladh, Wavelength dependence of extinction in sooting flat premixed flames in the visible and near-infrared regimes, *Appl. Phys. B: Lasers Opt.*, 2015, **119**(4), 657–667, DOI: 10.1007/s00340-015-6079-z.
- G. A. Kelesidis and S. E. Pratsinis, Determination of the volume fraction of soot accounting for its composition and morphology, *Proc. Combust. Inst.*, 2020, 1–8, DOI: 10.1016/j.proci.2020.07.055.
- F. Migliorini, K. A. Thomson and G. J. Smallwood, Investigation of optical properties of aging soot, *Appl. Phys. B: Lasers Opt.*, 2011, **104**(2), 273–283, DOI: 10.1007/s00340-011-4396-4.
- G. De Falco, *et al.*, Experimental and numerical study of soot formation and evolution in co-flow laminar partially premixed flames, *Fuel*, 2018, **220**, DOI: 10.1016/j.fuel.2018.02.028.
- H. A. Michelsen, Probing soot formation, chemical and physical evolution, and oxidation: A review of in situ diagnostic techniques and needs, *Proc. Combust. Inst.*, 2017, **36**(1), 717–735, DOI: 10.1016/j.proci.2016.08.027.
- P. Desgroux, X. Mercier and K. A. Thomson, Study of the formation of soot and its precursors in flames using optical diagnostics, *Proc. Combust. Inst.*, 2013, **34**(1), 1713–1738, DOI: 10.1016/j.proci.2012.09.004.
- F. Migliorini, S. De Iulii, S. Maffi, F. Cignoli and G. Zizak, Investigation on the influence of soot size on prompt LII



- signals in flames, *Appl. Phys. B: Lasers Opt.*, 2009, **96**(4), 637–643, DOI: 10.1007/s00340-009-3524-x.
- 19 S. Maffi, S. De Iuliis, F. Cignoli and G. Zizak, Investigation on thermal accommodation coefficient and soot absorption function with two-color TIRE-LII technique in rich premixed flames, *Appl. Phys. B: Lasers Opt.*, 2011, **104**(2), 357–366, DOI: 10.1007/s00340-011-4536-x.
- 20 S. De Iuliis, S. Maffi, F. Cignoli and G. Zizak, Three-angle scattering/extinction versus TEM measurements on soot in premixed ethylene/air flame, *Appl. Phys. B: Lasers Opt.*, 2011, **102**(4), 891–903, DOI: 10.1007/s00340-010-4344-8.
- 21 F. Cignoli, S. De Iuliis and G. Zizak, Soot tendency of diesel oil of different aromatic content as measured in rich premixed flames, in *International Symposium on Combustion Abstracts of Accepted Papers*, 2000, vol. 80, pp. 945–955.
- 22 F. Migliorini, S. De Iuliis, S. Maffi and G. Zizak, Environmental application of pulsed laser-induced incandescence, *Appl. Phys. B: Lasers Opt.*, 2013, **112**(3), 433–440, DOI: 10.1007/s00340-013-5385-6.
- 23 K. Wan, X. Shi and H. Wang, Quantum confinement and size resolved modeling of electronic and optical properties of small soot particles, *Proc. Combust. Inst.*, 2020, 1–8, DOI: 10.1016/j.proci.2020.07.145.
- 24 C. Liu, *et al.*, Flame-formed carbon nanoparticles exhibit quantum dot behaviors, *Proc. Natl. Acad. Sci. U. S. A.*, 2019, **116**(26), 12692–12697, DOI: 10.1073/pnas.1900205116.
- 25 C. Russo, B. Apicella and A. Ciajolo, Blue and green luminescent carbon nanodots from controllable fuel-rich flame reactors, *Sci. Rep.*, 2019, **9**(1), 1–8, DOI: 10.1038/s41598-019-50919-1.
- 26 H. A. Michelsen, C. Schulz, G. J. Smallwood and S. Will, Laser-induced incandescence: Particulate diagnostics for combustion, atmospheric, and industrial applications, *Prog. Energy Combust. Sci.*, 2015, **51**, 2–48, DOI: 10.1016/j.pecc.2015.07.001.
- 27 G. De Falco, *et al.*, Electronic band gap of flame-formed carbon nanoparticles by scanning tunneling spectroscopy, *Proc. Combust. Inst.*, 2020, 1–8, DOI: 10.1016/j.proci.2020.07.109.
- 28 F. Migliorini, S. De Iuliis, R. Dondè, M. Commodo, P. Minutolo and A. D'Anna, Nanosecond laser irradiation of soot particles: Insights on structure and optical properties, *Exp. Therm. Fluid Sci.*, 2020, **114**, DOI: 10.1016/j.expthermflusci.2020.110064.
- 29 J. Tauc, R. Grigorovici and A. Vancu, Optical properties and electronic structure of amorphous germanium, *Phys. Status Solidi B*, 1966, **15**, 627–637, DOI: 10.1002/pssb.19660150224.
- 30 J. Robertson, Hard amorphous (diamond-like) Carbon, *Prog. Solid State Chem.*, 1991, **21**, 199–333, DOI: 10.1016/0079-6786(91)90002-H.
- 31 J. Robertson, Amorphous carbon, *Curr. Opin. Solid State Mater. Sci.*, 1996, **1**(4), 557–561, DOI: 10.1016/S1359-0286(96)80072-6.
- 32 P. Minutolo, G. Gambu and A. D'Alessio, UV-visible absorption spectra of rich premixed flames, in *Twenty-sixth Symposium (International) on Combustion*, 1996, pp. 951–957.
- 33 C. Russo, *et al.*, Optical band gap analysis of soot and organic carbon in premixed ethylene flames: Comparison of *in situ* and *ex situ* absorption measurements, *Carbon*, 2020, **158**, 89–96, DOI: 10.1016/j.carbon.2019.11.087.
- 34 E. M. Adkins and J. H. Miller, Extinction measurements for optical band gap determination of soot in a series of nitrogen-diluted ethylene/air non-premixed flames, *Phys. Chem. Chem. Phys.*, 2015, **17**(4), 2686–2695, DOI: 10.1039/c4cp04452e.
- 35 F. Liu and G. J. Smallwood, Effects of detection wavelengths on soot volume fraction measurements using the auto-compensating LII technique, *Combust. Sci. Technol.*, 2019, DOI: 10.1080/00102202.2019.1678837.
- 36 S. De Iuliis, F. Cignoli and G. Zizak, Two-color laser-induced incandescence (2C-LII) technique for absolute soot volume fraction measurements in flames, *Appl. Opt.*, 2005, **44**(34), 7414–7423, DOI: 10.1364/AO.44.007414.
- 37 S. De Iuliis, F. Cignoli, S. Maffi and G. Zizak, Influence of the cumulative effects of multiple laser pulses on laser-induced incandescence signals from soot, *Appl. Phys. B: Lasers Opt.*, 2011, **104**(2), 321–330, DOI: 10.1007/s00340-011-4535-y.
- 38 F. Migliorini, S. De Iuliis, S. Maffi and G. Zizak, Saturation curves of two-color laser-induced incandescence measurements for the investigation of soot optical properties, *Appl. Phys. B: Lasers Opt.*, 2015, **120**(3), 417–427, DOI: 10.1007/s00340-015-6151-8.
- 39 A. D'Alessio, A. D'Anna, G. Gambi and P. Minutolo, The spectroscopic characterisation of UV absorbing nanoparticles in fuel rich soot forming flames, *J. Aerosol Sci.*, 1998, **29**(4), 397–409, DOI: 10.1016/S0021-8502(97)00457-6.
- 40 R. C. Millikan, Optical properties of soot, *J. Opt. Soc. Am.*, 1961, **51**, 698–699, DOI: 10.1364/JOSA.51.000698.
- 41 E. A. Davis and N. F. Mott, Conduction in non-crystalline systems V. Conductivity, optical absorption and photoconductivity in amorphous semiconductors, *Philos. Mag.*, 1970, **22**, 0903–0922, DOI: 10.1080/14786437008221061.
- 42 D. Chen and H. Wang, HOMO–LUMO energy splitting in polycyclic aromatic hydrocarbons and their derivatives, *Proc. Combust. Inst.*, 2019, **37**(1), 953–959, DOI: 10.1016/j.proci.2018.06.120.
- 43 S. De Iuliis, F. Migliorini, F. Cignoli and G. Zizak, Peak soot temperature in laser-induced incandescence measurements, *Appl. Phys. B: Lasers Opt.*, 2006, **83**(3), 397–402, DOI: 10.1007/s00340-006-2210-5.
- 44 S. Bejaoui, S. Batut, E. Therssen, N. Lamoureux, P. Desgroux and F. Liu, Measurements and modeling of laser-induced incandescence of soot at different heights in a flat premixed flame, *Appl. Phys. B: Lasers Opt.*, 2015, **118**(3), 449–469, DOI: 10.1007/s00340-015-6014-3.
- 45 H. Bladh, J. Johnsson, N.-E. Olofsson, A. Bohlin and P.-E. Bengtsson, Optical soot characterization using two-color laser-induced incandescence (2C-LII) in the soot growth region of a premixed flat flame, *Proc. Combust. Inst.*, 2011, **33**, 641–649, DOI: 10.1016/j.proci.2010.06.166.
- 46 E. V. Gurentsov, A review on determining the refractive index function, thermal accommodation coefficient and evaporation temperature of light-absorbing nanoparticles suspended in the



- gas phase using the laser-induced incandescence, *Nanotechnol. Rev.*, 2018, **7**(6), 583–604, DOI: 10.1515/NTREV-2018-0080.
- 47 H. A. Michelsen, Effects of maturity and temperature on soot density and specific heat, *Proc. Combust. Inst.*, 2020, 1–9, DOI: 10.1016/j.proci.2020.06.383.
- 48 F. Liu, S. Rogak, D. R. Snelling, M. Saffaripour, K. A. Thomson and G. J. Smallwood, Effect of laser fluence non-uniformity on ambient-temperature soot measurements using the auto-compensating laser-induced incandescence technique, *Appl. Phys. B: Lasers Opt.*, 2016, **122**, 286, DOI: 10.1007/s00340-016-6553-2.
- 49 A. V. Eremin, E. V. Gurentsov and R. N. Kolotushkin, The change of soot refractive index function along the height of premixed ethylene/air flame and its correlation with soot structure, *Appl. Phys. B: Lasers Opt.*, 2020, **126**, 125, DOI: 10.1007/s00340-020-07426-3.

